Fast Track Communications
IOP Publishing
Plasma Sources Science and Technology
Plasma Sources Sci. Technol. **24** (2015) 032003 (4pp)
doi:10.1088/0963-0252/24/3/032003

Fast Track Communication

Observation of high-frequency ion instabilities in a cross-field plasma

Julien Vaudolon and Stéphane Mazouffre

ICARE—CNRS, 1C Avenue de la Recherche Scientifique, 45071 Orléans Cedex 2, France

E-mail: julien.vaudolon@cnrs-orleans.fr and stephane.mazouffre@cnrs-orleans.fr

Received 24 February 2015, revised 16 April 2015
Accepted for publication 14 May 2015
Published 1 June 2015

Abstract

This paper reports on the examination of the high-frequency ion dynamics in a low-pressure cross-field plasma. Measurements of the time-varying ion velocity distribution function were carried out by photon-counting laser-induced fluorescence spectroscopy. A temporal correlation was found between the low-frequency ionization process and the high frequency ion instability. The high-frequency spectral properties of the ion mean velocity are compared with a perturbed fluid model of the plasma flow on the source axis. The wavelength of the high-frequency mode is similar to the electric field extent outside the cavity. Surprisingly the mode appears only in the area of negative magnetic field gradient.

Keywords: Hall thruster, laser-induced fluorescence, instability

(Some figures may appear in colour only in the online journal)

Low-pressure cross-field plasma sources are characterized by a broad family of oscillatory phenomena [1]. Despite decades of research, many properties of these oscillations are still poorly-understood [2]. However, knowledge of the instability characteristics is key for describing plasma processes, such as the anomalous electron transport, ionization and ion acceleration. While many experimental and numerical studies have focused on ionization instabilities in the kHz range and on electron turbulence in the MHz range [3–6], experimental work on the intermediate frequency band instabilities remains rare. While a wide variety of models has been developed, no experimental validation supports their outcomes [7, 8]. In Hall thrusters, this intermediate range of oscillations between 100 kHz and 1 MHz is oft-referred to as the ion transit-time (ITT) instability, because the typical time period is on the order of the ion time-of-flight through the acceleration region. The practical difficulty of accessing the ion dynamics over a very short time scale, without perturbing the plasma, has made knowledge of the fundamental properties of the ITT difficult to obtain.

The present paper reports on the first direct evidence of the ITT instability in a cross-field plasma accelerator. The measurements, associated with a two-fluid model of the plasma, reveal complex physics which is dependent on the low frequency ionization mode and the magnetic field profile.

Progress towards a better understanding of this instability requires a tailored diagnostic technique with high spatial and temporal resolution. Time-resolved laser-induced fluorescence (TR-LIF) measurements of the local ion velocity distribution function (IVDF) oscillations are made with a resolution of 10 MHz. The LIF principle is to access the velocity of probed particles along a laser beam direction by measuring the Doppler shift of absorbed photons. The experimental procedure and apparatus have been described elsewhere [9]. In short, the metastable Xe II ion transition $5d^2F_{7/2} \rightarrow 6p^2D_{5/2}$ at 834.9527 nm is pumped by a laser diode. A feedback loop keeps the laser frequency constant during an acquisition. The wavemeter uncertainty is 80 MHz, which corresponds to an ion velocity uncertainty of 60 m s^{-1}. Via a high gain low dark noise photomultiplier tube (PMT) and monochromator, the fluorescence radiation at 541.9 nm is recorded. The spatial resolution is 200 μm . The PMT signal is discriminated and amplified. A multichannel scaler then records the counting rate of events, i.e. the fluorescence photon arrival. The

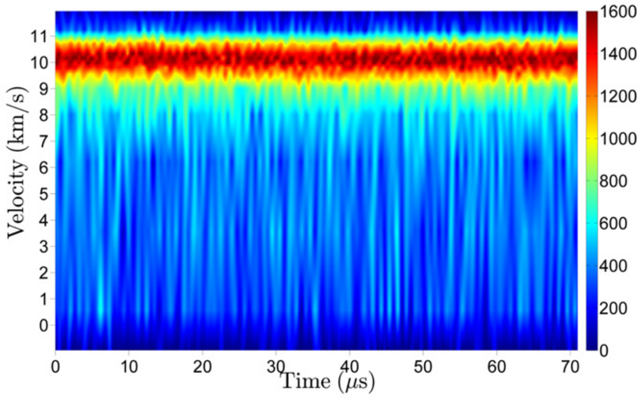

Figure 1. High frequency oscillations of the IVDF at 3 mm downstream the exit plane during a breathing oscillation. The colorbar indicates the number of fluorescence photons. Each ion velocity group has been probed during approximately 5 min, through 176 000 acquisitions on 7150 bins of the counting card.

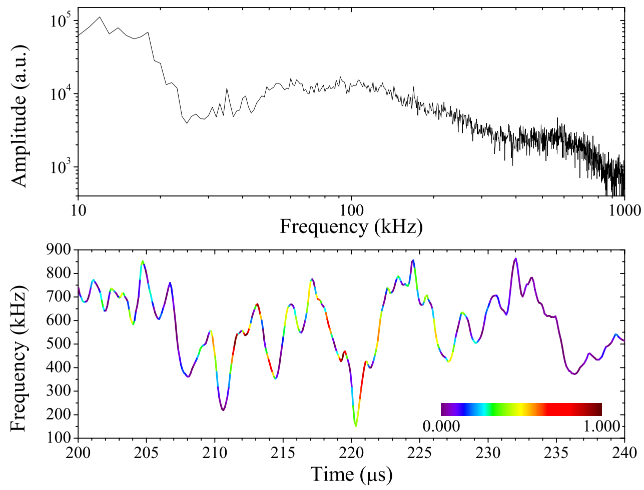

Figure 2. Marginal and Hilbert spectra of the ion mean velocity oscillation at $z = 1$ mm: (top) marginal spectrum; (bottom) oscillation at 575 kHz. The colorbar indicates the normalized power level.

temporal resolution is 100 ns. Fifteen wavelengths that best describe the time-averaged IVDF are chosen to yield the time-dependent IVDF. Time coherence is ensured by modulating the discharge current at a low-frequency resonance originating from the ionization process, and referred to as the *breathing mode* [5]. A coherent behavior of the discharge has been obtained at a modulation frequency of 14 kHz. Synchronizing the discharge modulation and the acquisitions allows for averaging over a very large number of cycles, which ensures a high signal-to-noise ratio. Notice that the modulation of the plasma breathing oscillations has been shown not to perturb the time-averaged behavior of the discharge, unlike previous techniques that relied on periodic and short discharge power cuts [9, 10]. This diagnostic technique has been successfully used to observe the low-frequency oscillations of the electric field that is established in these plasmas [11].

The source used in this study is a Hall thruster, used for in-space propulsion of satellites and exploration probes. The source has been described in a previous work [12]. It consists in a low-pressure $\mathbf{E} \times \mathbf{B}$ discharge generated between an anode, placed at the upstream end of an annular ceramic cavity, and an external hollow cathode. The magnetic field is generated by SmCo magnets. The typical field strength is around a hundred Gauss, so that the electrons are magnetized while the more massive ions are not. The discharge voltage is 200 V. Xe has been used as a working gas. The anode mass flow rate is 1 mg s^{-1} and the cathode mass flow rate is 0.2 mg s^{-1}. The source is electrically floating, which mimics the flight mode operation. Axial IVDFs, $f(\mathbf{x}, v_z, t)$, have been recorded along the source channel axis, from -13 mm up to 10 mm, where the position 0 mm is the cavity exit plane. Due to the annular geometry of the source, we use a (r, θ, z) cylindrical coordinate system.

Figure 1 shows the raw IVDF recorded at $z = 3$ mm away from the source cavity for frequencies below 1 MHz, and illustrates the measurement outcome. The number of fluorescence photons is acquired as a function of both the ion velocity and time during a breathing oscillation. Each ion velocity group has been probed during approximately 5 min, through 176 000 acquisitions on 7150 bins of the counting card. Evidence of low frequency IVDF oscillations can be found elsewhere [11]. Oscillations of the IVDF at a few hundreds of kHz are revealed for the first time. Low- and high-frequency oscillations of the IVDF have been observed at every measurement location.

The Hilbert–Huang spectral analysis has been applied to the measured time series [13, 14]. Unlike Fourier transform, this technique is well-suited for the study of non-stationary and non-linear signals. Based on the Huang sifting algorithm, the Hilbert spectral method allows the computation of the Hilbert and frequency spectra of a signal. The frequency spectrum is called a *marginal spectrum* in the Hilbert spectral technique [13, 14]. These spectra are somewhat similar to a Fourier spectrum, with the additional contribution of the time-dependent nature of the frequency content.

The spectral analysis outcome is exemplified in figure 2. The marginal spectrum of the ion mean velocity at 1 mm downstream the source exit plane is shown. The marginal spectrum reveals three distinct regimes. The breathing mode contains the main part of the energy at 10–20 kHz. Two other oscillating regimes are centered at 100 kHz and 575 kHz. The Hilbert spectrum of the latter oscillation is shown in the figure lower part. The intermittent nature of this regime is clearly seen. It justifies the application of the Hilbert–Huang technique. Structures that contain a significant amount of energy are observed above 100 kHz while the time coherence is based on stabilizing a low frequency mode of the discharge at 14 kHz. Whether the link between the low and high frequency oscillations happens naturally in Hall thrusters, or is influenced by the oscillatory driving of the discharge remains unknown though. The results of figure 2, and examples of coherent structures obtained through the Hilbert–Huang analysis that can be found in [11], show that the ion dynamics in the [100 kHz; 1 MHz] band is either controlled and stabilized by the breathing mode, or influenced by the modulation apparatus.

While the low frequency oscillations are well-understood, the transit time instability description has not progressed much from an experimental viewpoint since the early work of Esipchuk and Morozov in 1973 [15], rendering the comparison with fluid models impossible. Observations of the floating plasma potential reported at that time an instability, occurring at a frequency corresponding to the reciprocal ion time-of-flight through the acceleration zone, $f \approx v_z/L$, with a wide spread in frequency so that $\Delta f \approx f$.

The marginal spectrum of the time-resolved ion mean velocity has been computed at each measurement location, which allows to detect the existence of the instability, and ultimately to compute its frequency content. In order to extract more information from the measured IVDF, we correlate the experimental observations to a linearised one-dimensional two-fluid model of the plasma, and determine the plasma parameters which influence the instability.

The plasma is assumed to be composed of cold unmagnetized ions and cold magnetized electrons. The magnetic field is assumed to be purely radial, which is a reasonable approximation on the cavity axis. We study the case of quasineutral perturbations, and dissipative and ionization processes are neglected. For the sake of simplicity, and for allowing the comparison of the theoretical results with the LIF data set, the model is one-dimensional. The electric field profile along the chamber axis has been obtained using the LIF measurements and a fluid computation [16]. Finally, we consider that the typical transit time frequency ω is much lower than the electron cyclotron frequency ω_{Be}, so that $\omega << \omega_{\text{Be}}$. Under these assumptions, the continuity equation and the momentum conservation equation for both the ions and the electrons are linearised and read

$$\begin{cases} \dfrac{\partial \tilde{n}}{\partial t} + n\dfrac{\partial \tilde{v}_z}{\partial z} + v_z\dfrac{\partial \tilde{n}}{\partial z} + \tilde{v}_z\dfrac{\partial n}{\partial z} + \tilde{n}\dfrac{\partial v_z}{\partial z} = 0, \\ \dfrac{\partial \tilde{v}_z}{\partial t} + v_z\dfrac{\partial \tilde{v}_z}{\partial z} + \tilde{v}_z\dfrac{\partial v_z}{\partial z} = -\dfrac{e}{m_{\text{i}}}\dfrac{\partial \tilde{\Phi}}{\partial z}, \\ \dfrac{\partial \tilde{n}}{\partial t} + n\dfrac{\partial \tilde{u}_z}{\partial z} + \tilde{u}_z\dfrac{\partial n}{\partial z} = 0, \\ \dfrac{\partial \tilde{u}_\theta}{\partial t} = \dfrac{e}{m_{\text{e}}}\tilde{u}_z B_r, \\ \dfrac{\partial \tilde{u}_z}{\partial t} = \dfrac{e}{m_{\text{e}}}\left(\dfrac{\partial \tilde{\Phi}}{\partial z} - \tilde{u}_\theta B_r\right), \end{cases} \tag{1}$$

where the subscripts r, θ and z refer to the cylindrical coordinates, v and u are the ion and electron velocities respectively, n is the plasma density, Φ the accelerating potential, e the ion charge, m_{i} the ion mass, m_{e} the electron mass and B_r the magnetic field. Perturbed quantities are labelled by a tilde superscript. We look for the solution of system (1) in Fourier form $\exp[\text{i}(kz - \omega t)]$ where $\mathbf{k} = (0, 0, k)$ is the perturbation wave-vector.

After a few manipulations, the dispersion relation is obtained in the form of (2), in which ω_{Bi} is the ion cyclotron frequency. Equation (2) has two complex roots. Only one of them has a positive real part and is therefore considered as the physical solution. The solution of the dispersion relation

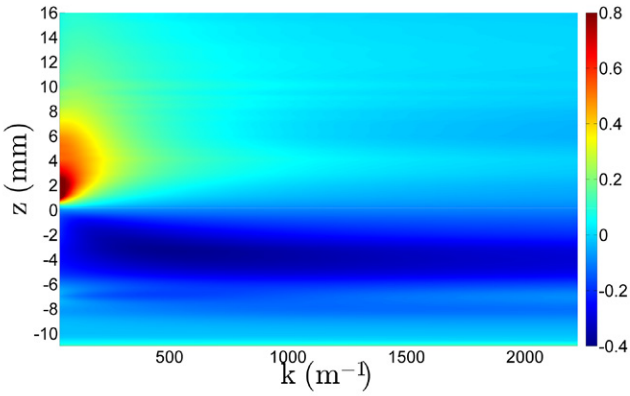

Figure 3. Growth rate mapping as a function of the mode wavenumber and axial position along the cavity axis. The colorbar is expressed in MHz.

is given by (3). In the remaining of the analysis, we write $\omega = \omega_r + \text{i}\gamma$ where ω_r is the mode frequency and γ is the growth rate of the instability.

$$\left(\frac{1}{v_z}\frac{\partial v_z}{\partial z} + \frac{2}{B_r}\frac{\partial B_r}{\partial z} - \text{i}k\right)\left(\frac{1}{v_z}\left[\text{i}\omega - \frac{\partial v_z}{\partial z}\right] - \text{i}k\right)^2 + \frac{\omega_{\text{Be}}\omega_{\text{Bi}}}{v_z^2}\left(\frac{1}{v_z}\frac{\partial v_z}{\partial z} - \text{i}k\right) = 0. \tag{2}$$

$$\omega = v_z k - \text{i}\left\{\frac{\partial v_z}{\partial z} + \left[\frac{\omega_{\text{Be}}\omega_{\text{Bi}}\left(\text{i}k - \frac{1}{v_z}\frac{\partial v_z}{\partial z}\right)}{\frac{1}{v_z}\frac{\partial v_z}{\partial z} + \frac{2}{B_r}\frac{\partial B_r}{\partial z} - \text{i}k}\right]^{\frac{1}{2}}\right\}. \tag{3}$$

The growth rate of the instability is mapped in figure 3, in MHz, as a function of the mode wavenumber and axial position along the cavity axis. Regions in which the growth rate is positive, and where unstable modes are therefore likely to appear, extend downstream the source exit plane, for $z > 1$ mm and $k < 1000$ m^{-1}. The corresponding wavelength is on the order of the width of the electric field distribution outside the cavity. The growth rate becomes negative for higher wavenumbers between $z = 4$–9 mm, which is the location of the high electric field region. Details concerning the electric field distribution in this source can be found in [11]. It is worth noting that the growth rate is negative for any wavenumber in regions where $z < 1$ mm, i.e. inside the cavity. Expanding the dispersion relation and factorizing by the powers of γ, it can be seen that, in our operating conditions, the sign of the growth rate is determined by the opposite sign of $\frac{\partial v_z}{\partial z} + 2\frac{v_z}{B_r}\frac{\partial B_r}{\partial z}$. Owing to the strong axial electric field, $\frac{\partial v_z}{\partial z} > 0$ at each location, and therefore the instability triggering is primarily determined by the magnetic field profile.

The mode frequencies are mapped in figure 4, in MHz, in the area of positive growth rate, as a function of the mode wavenumber and axial position along the cavity axis. The instability is more likely to occur at low wavenumbers, which scale with the acceleration zone length, on the order of 1 cm. In this region, frequencies range from 150 kHz to 1.2 MHz,

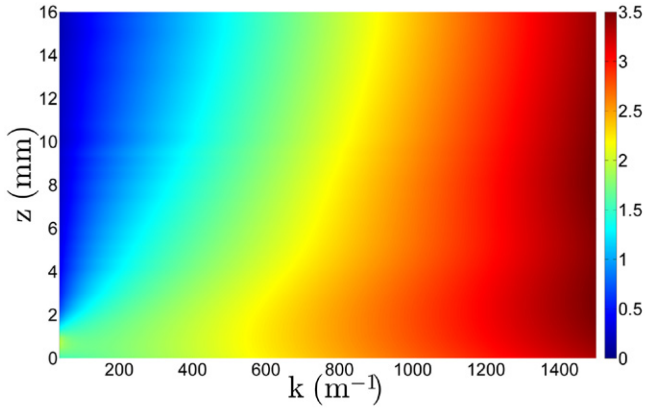

Figure 4. Colormap of the mode frequency as a function of wavenumber and axial location. The colorbar is expressed in MHz.

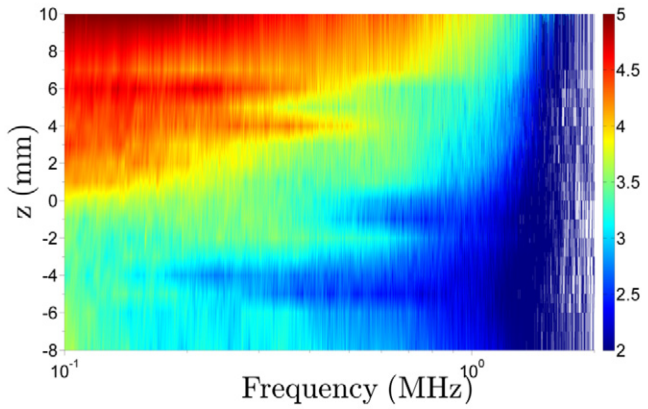

Figure 5. Marginal spectra of the measured ion mean velocity as a function of z. The colorbar is expressed in arbitrary units.

which is on the order of magnitude of the reciprocal ion time-of-flight through the device $\approx v_z/L$.

The marginal spectra of the measured ion mean velocity temporal evolution are presented in figure 5, as a function of the axial position along the cavity axis. The colorbar is expressed in arbitrary units. Agreement can be found between the experimental results and the analytical results. The order of magnitude of the mode frequency indeed appears to be similar, ranging in the 100 kHz–1.1 MHz band. Notice that the experimental results confirm the turbulent nature of the instability first reported by Esipchuk and Morozov [15], i.e. the frequency spread is on the same order of magnitude as the frequency scale : $\Delta f \approx f$. A noticeable feature can be found in figure 5. The amplitude of the unstable mode increases rapidly outside the cavity. This picture is in agreement with the growth rate profile analyzed previously, which indicates that the magnetic field profile may indeed be a key element for describing the instability occurrence.

The first experimental description of the high frequency ion dynamics in a low-pressure cross-field plasma with high spatial and temporal resolution has been reported. The TR-LIF technique, based on a photon-counting method and active stabilization of the discharge behavior, shows that the high frequency ion properties of the plasma are influenced by the lower frequency breathing mode, or by the modulation of the keeper electrode. The properties of the ion mean velocity have been compared with a one-dimensional two-fluid model. The ion transit-time oscillation appears only in the region of negative magnetic field gradient both analytically and experimentally. Additionally, its wavelength appears to be similar to the electric field distribution extent outside the cavity.

Acknowledgments

The authors would like to thank S Tsikata for stimulating discussions and T André for his assistance in numerical matters. J Vaudolon benefits from a CNES-Snecma PhD grant.

References

[1] Choueiri E Y 2001 Plasma oscillations in Hall thrusters *Phys. Plasmas* **8** 1411
[2] Zhurin V V, Kaufman H R and Robinson R S 1999 Physics of closed drift thrusters *Plasma Sources Sci. Technol.* **8** R1
[3] Ellison C L, Raitses Y and Fisch N J 2012 Cross-field electron transport induced by a rotating spoke in a cylindrical Hall thruster *Phys. Plasmas* **19** 013503
[4] Tsikata S, Honoré C and Grésillon D 2013 Collective Thomson scattering for studying plasma instabilities in electric thrusters *J. Instrum.* **8** C10012
[5] Boeuf J P and Garrigues L 1998 Low frequency oscillations in a stationary plasma thruster *J. Appl. Phys.* **84** 3541
[6] Brenning N, Lundin D, Minea T, Costin C and Vitelaru C 2013 Spokes and charged particle transport in HiPIMS magnetrons *J. Phys. D: Appl. Phys.* **46** 084005
[7] Barral S, Makowski K, Peradzyński Z and Dudeck M 2005 Transit-time instability in Hall thrusters *Phys. Plasmas* **12** 073504
[8] Kapulkin A, Behar E and Raitses Y 2013 Ion beam instability in Hall thrusters *Proc. of the 33rd Int. Electric Propulsion Conf.* (*Washington, DC, USA*)
[9] Vaudolon J, Balika L and Mazouffre S 2013 Photon counting technique applied to time-resolved laser-induced fluorescence measurements on a stabilized discharge *Rev. Sci. Instrum.* **84** 073512
[10] Mazouffre S and Bourgeois G 2010 Spatio-temporal characteristics of ion velocity in a Hall thruster discharge *Plasma Sources Sci. Technol.* **19** 065018
[11] Vaudolon J, Khiar B and Mazouffre S 2014 Time evolution of the electric field in a Hall thruster *Plasma Sources Sci. Technol.* **23** 022002
[12] Mazouffre S, Bourgeois G, Dannenmayer K and Lejeune A 2012 Ionization and acceleration processes in a small, variable channel width, permanent-magnet Hall thruster *J. Phys. D: Appl. Phys.* **45** 185203
[13] Huang N E and Wu Z 2008 A review on Hilbert–Huang transform: method and its applications to geophysical studies *Rev. Geophys.* **46** 1–23
[14] Kurzyna J, Mazouffre S, Lazurenko A, Albaréde L, Bonhomme G, Makowski K, Dudeck M and Peradzyński Z 2005 Spectral analysis of Hall-effect thruster plasma oscillations based on the empirical mode decomposition *Phys. Plasmas* **12** 123506
[15] Esipchuk Yu V, Morozov A I, Tilinin G N and Trofimov A V 1973 Plasma oscillations in closed-drift accelerators with an extended acceleration zone *Zh. Tekh. Fiz.* **43** 1466–73
[16] Vaudolon J and Mazouffre S 2014 Indirect determination of the electric field in plasma discharges using laser-induced fluorescence spectroscopy *Phys. Plasmas* **21** 093505